Direct Laser Acceleration in Underdense Plasmas with Multi-PW Lasers: A Path to High-Charge, GeV-Class Electron Bunches

R. Babjak,[1,2,*] L. Willingale,[3] A. Arefiev,[4] and M. Vranic[1]

[1]GoLP/Instituto de Plasmas e Fusão Nuclear, Instituto Superior Técnico, Universidade de Lisboa, Lisbon 1049-001, Portugal
[2]Institute of Plasma Physics, Czech Academy of Sciences, Za Slovankou 1782/3, 182 00 Praha 8, Czechia
[3]Gérard Mourou Center for Ultrafast Optical Sciences, University of Michigan, Ann Arbor, Michigan 48109, USA
[4]University of California San Diego, La Jolla, California 92093, USA

(Received 21 April 2023; revised 22 January 2024; accepted 27 February 2024; published 22 March 2024)

The direct laser acceleration (DLA) of electrons in underdense plasmas can provide hundreds of nC of electrons accelerated to near-GeV energies using currently available lasers. Here we demonstrate the key role of electron transverse displacement in the acceleration and use it to analytically predict the expected maximum electron energies. The energy scaling is shown to be in agreement with full-scale quasi-3D particle-in-cell simulations of a laser pulse propagating through a preformed guiding channel and can be directly used for optimizing DLA in near-future laser facilities. The strategy towards optimizing DLA through matched laser focusing is presented for a wide range of plasma densities paired with current and near-future laser technology. Electron energies in excess of 10 GeV are accessible for lasers at $I \sim 10^{21}$ W/cm^2.

DOI: 10.1103/PhysRevLett.132.125001

Advanced acceleration schemes for electrons in plasmas allow us to obtain multi-GeV electron bunches within a few centimeters of propagation. The most frequently explored scheme thus far is laser-wakefield acceleration (LWFA) [1–4], with 7.8 GeV maximum energy achieved to date [5]. One disadvantage of the LWFA is that it provides a relatively low number of accelerated electrons (tens of pC). Many applications such as x-ray and gamma-ray generation [6–9], ion acceleration [10,11], or electron-positron pair creation [12–17] would benefit from having a high charge electron bunch, but do not require mono-energetic electrons. For those applications, direct laser acceleration (DLA) [18,19] is a promising alternative to provide the electron charge on the order of hundreds of nC [20,21]. In plasmas, DLA and LWFA can act simultaneously [22–27] and in a recent experiment the obtained electron beams had energies exceeding 10 GeV [28]. DLA could provide an opportunity to achieve an efficient energy transfer from the available laser energy into energetic electrons in the upcoming 10 PW-class laser facilities [29–31]. According to experimental and simulation results so far, the electron energies are expected to vary as a function of the plasma density [20,32–44]. As the propagation of the laser pulse through the plasma is highly nonlinear and has a significant impact on the acceleration, obtaining a direct comparison of theory, particle-in-cell (PIC) simulations, and experiments is a challenging task. Previous theoretical models of DLA therefore use a simplified analytical description of the acceleration to predict the electron energies depending on the laser a_0 and the plasma density in ideal conditions (e.g., a plane-wave laser) [45].

In this Letter, we propose a new model for predicting electron energies. We uncover the key role of the laser width in obtaining an efficient DLA acceleration, which allows us to propose optimal laser focusing to achieve the maximum electron energy gain. Even though higher laser intensities generally provide higher electron energy within a shorter propagation distance, the relation between the laser intensity and the electron energy cutoff is not linear, and we show that going for the highest possible laser intensity may not be the most favorable approach. Within an ion channel, particles perform betatron oscillations with a certain amplitude. An electron can experience a resonant energy gain when the frequency of these oscillations matches the frequency of the laser field oscillations at the electron location. Our analytical model predicts the maximum resonant amplitude for a given laser intensity. This uncovers a trade-off between using a highest possible laser intensity and a spot size with a large enough interaction volume for optimal acceleration to occur. Our findings (both analytical and from PIC simulations) show that using a not-so-tight focus ($\sim 10\lambda$) provides higher electron energies compared with when the same laser pulse is focused close to the diffraction limit. This comes with an added benefit that the stable laser guiding is easier to achieve for paraxial laser beams. We can expect to accelerate electrons of > hundreds nC charge to multi-GeV energies within millimeters or centimeters of plasma.

The most favorable conditions for electron acceleration using DLA are when a long laser pulse (hundreds of fs) propagates through an underdense or near-critical plasma.

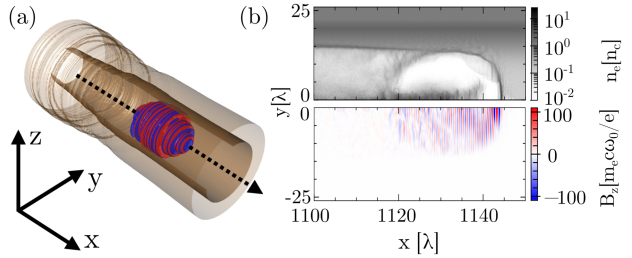

FIG. 1. (a) Schematic representation of the laser pulse propagating through the preformed guiding channel. (b) Electron density during the interaction of the 10 PW laser pulse focused to $a_0 = 85$ interacting with the channel with the density at the center $n_e = 0.1 n_c$ and the laser pulse transverse magnetic field component after ≈1 mm of propagation.

The ponderomotive force expels the electrons creating an ion channel, see Fig. 1(a). Quasistatic electromagnetic fields are generated within the ion channel, facilitating electron oscillations around the central axis and causing some electrons to be resonantly accelerated to energies exceeding the vacuum limit. The simplest description of DLA assumes the laser is a plane wave with a temporal envelope propagating within the static electric and magnetic fields linearly dependent on the radial distance (see Appendix) [19,45–48]. In this ideal description, the equations have a conserved quantity $I = \gamma - p_x/m_e c + \omega_p^2 y^2/4c^2$ throughout the interaction [45], as long as there are no losses (e.g., radiation reaction [49]) and the background plasma parameters remain constant. Here, ω_p stands for the background plasma frequency, y is the transverse displacement of the oscillating electron, γ is the relativistic Lorentz factor, and p_x is the momentum in the direction of laser propagation. The integral of motion I can be derived directly from the Hamiltonian. The plasma channel has a radial electric field and an azimuthal magnetic field, both acting on negatively charged particles copropagating with the laser in the direction towards the channel axis [45,50–52]. This causes betatron oscillations with a typical frequency $\omega_\beta = \omega_p/\sqrt{2\gamma}$ [53]. Electrons simultaneously oscillate in the field of the laser, which is modeled as a wave packet with the angular frequency ω_0. As relativistic electrons copropagate with a laser, the resonant DLA sets off if the frequency of the laser field oscillations at the electron location ω' matches the frequency of the betatron oscillations. The theoretical maximum energy of the most energetic electrons is then determined according to their initial position and the background plasma density [45]

$$\gamma_{\max} \simeq 2I^2 \frac{\omega_0^2}{\omega_p^2}. \tag{1}$$

Equation (1) represents the upper limit for the energy that an electron with given initial conditions can reach. Typically, the electrons with large oscillation amplitudes achieve the highest energies for a given plasma density n_p. The exact solution for all the electrons can be found in [45]. Once the maximum energy $\gamma_{\max}$ is achieved, an electron may decelerate due to the dephasing. For electrons starting with no transverse momentum, the maximum energy is fully determined by the background plasma frequency ω_p and the initial transverse distance from the axis y_0. If an electron has a finite initial p_{y0}, equivalent y_0 can always be found such that the particle has the same value of I (y_0 then represents the first oscillation amplitude possibly higher than the initial distance).

Whether the electron gets accelerated depends also on the nonlinear amplification condition $a_0\omega_p/(\omega_0 I^{3/2}) > \varepsilon_{cr}$ [45,54], where a_0 is the dimensionless field amplitude and ε_{cr} is the threshold parameter on the order of unity that varies depending on the electron pre-acceleration and the phase of the laser field where electron gets into the resonance. In the literature, the parameter takes values between 0.1 and 1.4, depending on the initial conditions and assumptions [45,46,54]. We introduce a new interpretation of the amplification condition that connects the laser intensity and the plasma density with the maximum resonant transverse amplitude:

$$y_{\max} = \frac{2c}{\omega_p}\sqrt{\left(\frac{a_0\omega_p}{\varepsilon_{cr}\omega_0}\right)^{2/3} - 1}. \tag{2}$$

Equation (2) assumes no pre-acceleration ($\gamma - p_x \approx 1$, $p_{y0} = 0$). It explicitly shows that a higher a_0 allows for the acceleration of electrons initially further from the channel axis when interacting with a plane wave. This allows higher intensity lasers to accelerate electrons to higher energies, even though according to Eq. (1), the maximum energy does not depend explicitly on a_0.

To verify the validity of Eq. (2) while neglecting effects such as self-focusing, superluminal phase velocity [55], or the effects arising from the finite width of focused laser pulse [56], we first numerically integrate the equations of motion for an electron in an idealized ion channel with given initial conditions ω_p/ω_0 and y_0. The pulse is modeled as a transverse plane wave with a short longitudinal ramp-up followed by a constant field amplitude. The ω_p/ω_0 determines the strength of the channel field that is expressed as $E_y^{ch} = m_e\omega_p^2 y/2e$. Without the loss of generality, we consider only the electric component of the channel field. The restitution force provided by the channel background is equivalent if it is composed of an azimuthal magnetic field, a radial electric field, or the combination of both $\vec{E}$ and $\vec{B}$ [49]. Along with the plasma frequency ω_p, the second varied initial parameter is the transverse oscillation amplitude y_0. We tracked the particles for ≈6300 laser periods (20 ps for a laser with $\lambda = 1$ μm) and extracted the maximum energy of each electron along its trajectory.

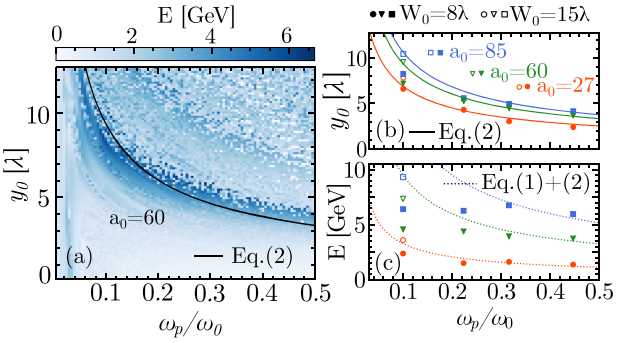

FIG. 2. (a) Maximum energies achieved for test particles, scanning different initial values of y_0 and ω_p/ω_0. The highest energies are achieved at the maximum resonance distance $y_{\max}$ given by Eq. (2). (b) Maximum expected distance of resonant electrons according to Eq. (2) for different laser intensities compared with the measured maximum resonant distance in quasi-3D PIC simulations. (c) Maximum energies observed in quasi-3D PIC simulations compared with the scaling given by combining Eqs. (1) and (2).

The results for laser $a_0 = 60$ are shown in Fig. 2(a). The black line represents Eq. (2), which predicts the maximum initial distance of electrons that are expected to achieve resonant motion. The resonance in test particle simulations (initial position y_0 where the maximum energy is obtained since $\gamma_{\max} \sim y_0^4$) is in excellent agreement with the parameter space expected from the analytical description in Eq. (2) if we take $\varepsilon_{cr} = 0.2$. Resonance can happen also in higher harmonics, which we observe for electrons accelerated further than the $y_{\max}$ but the energy gain is significantly lower for these cases. It is important to emphasize that there is a maximum initial transverse distance for resonant acceleration even during the interaction with a laser modeled as a transversely plane wave, which indicates that this is a fundamental property of the acceleration mechanism and not an effect of the channel or laser transverse dimension. In other words, it is beneficial to have a laser pulse wider than the maximum transverse resonant distance given by Eq. (2), but a further widening of the laser beam $W_0 \gg y_{\max}$ should not result in particle acceleration at a higher transverse oscillation amplitude.

The central role of $y_{\max}$ for the acceleration was also verified by the quasi-3D OSIRIS PIC simulations using a finite laser pulse propagating in a preformed plasma channel [57,58]. The transverse density structure of a guiding plasma channel prevents the laser pulse from defocusing and enables the propagation of the laser pulse for distances exceeding the Rayleigh length. The creation of structures that enable guiding of the laser pulse over several mm was previously studied both using PIC simulations and experimentally [59–61]. Please note that both preformed quasi-neutral plasma channel and an ion channel created by the laser pulse itself can guide the laser, but the effective interaction plasma density can be different for the two cases. The laser pulse with the Gaussian transverse profile with $W_0 = 8$ μm and the 200 fs duration interacts with the plasma for ≈1600 laser periods (5.3 ps, 1.6 mm) or longer if more time is needed to achieve maximum energies. The laser power is 1, 5, and 10 PW corresponding to the peak a_0 of 27, 60, and 85, respectively. The simulation details are provided in the Appendix. The laser B field and electron density are shown in Fig. 1(b).

The transverse oscillation amplitude of maximum energy electrons is extracted from phase space diagnostic in PIC simulations. Results summarized in Fig. 2(b) are compared with the expected values of $y_{\max}$ according to Eq. (2). The values observed in PIC simulation are in excellent agreement with our predictions except for the lowest density case of $n_e = 0.01 n_c$. The reason for the discrepancy is the fact that the laser pulse was not wide enough for the electrons to get into the resonance at the maximum transverse oscillation amplitude allowed for the considered a_0 values (i.e., $W_0 < y_{\max}$). Additional simulations performed with a wider spotsize ($W_0 = 15$ μm) represented with the same color using empty markers instead of full ones agreed with Eq. (2).

We have thus shown that we are able to predict the maximum transverse distance from the axis of resonant electrons. This can be used to predict the energies of such electrons. We first calculate $y_{\max}$ predicted by Eq. (2), and then use it to obtain $I_{\max} \approx 1 + \omega_p^2 y_{\max}^2/4c^2$. Placing the result in Eq. (1) gives the maximum energy and in a compact form can be written as

$$\gamma_{\max}^{\text{res}} = 2\left(\frac{a_0}{\varepsilon_{cr}}\right)^{4/3}\left(\frac{n_e}{n_c}\right)^{-1/3}. \tag{3}$$

The prediction is valid only if the laser pulse is wide enough and its propagation is stable for long enough to fully complete the acceleration. Using the acceleration rate over time from [49], the acceleration distance needed to achieve the energy $\gamma_{\max}^{\text{res}}$ is $L_{\text{acc}}/\lambda = 0.78 a_0^{2/3} \varepsilon_{cr}^{-5/3} (n_e/n_c)^{-2/3}$.

The prediction of the maximum energy for a given a_0 according to the above procedure is depicted by the lines in Fig. 2(c). They are compared with maximum energies achieved in corresponding PIC simulations (shown as points). A higher value of a_0 enables particles to achieve resonance at a bigger $y_{\max}$, and indirectly leads to higher electron energies.

Note, that both theoretical predictions and PIC simulations neglect the radiation reaction. The energy is not only limited by Eq. (1) but also by the radiation reaction energy losses [49]. For moderate laser field amplitudes used in our simulations the field of the ion channel is the dominant source of the radiation damping. The radiation limit for electron energy is proportional to $\gamma_{rr} \sim (\lambda a_0 \omega_0^2/(\omega_p^2 \sqrt{I}))^{2/5}$, and is more important for denser plasmas.

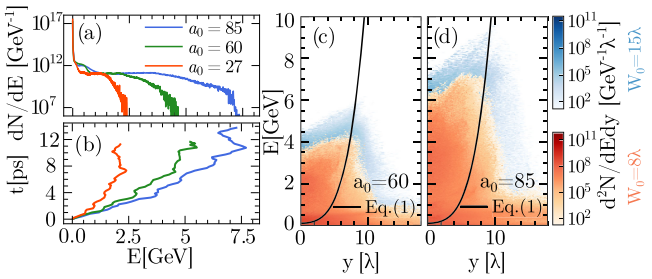

FIG. 3. (a) Distribution function of electrons after the maximum cutoff energy is achieved. (b) Maximum energy (in the simulation) over time. The acceleration stops after accomplishing the theoretical maximum energy associated with the amplitude y_0. (c)–(d) Electron distribution in energy and instantaneous distance from the axis y (not the same as y_0 as for most of electrons y can be midoscillation). Each panel shows electrons accelerated by lasers with different intensities, but the same spot size, where in (c) $W_0 = 8$ (d) $W_0 = 15$ μm. The background plasma density is $n_e = 0.01 n_c$ for all panels. Increasing a_0 resulted in electron acceleration further from the axis, and consequently higher maximum energies. Increasing the spot size had a similar effect.

Figure 3(a) shows the energy spectrum of the electrons at the moment when the acceleration was complete by reaching the maximum allowed energy given by Eq. (1). The broadband energy spectrum is characteristic for the DLA. The charge contained within the beam can be defined as the number of electrons with energies higher than the vacuum limit given by the $\gamma_{\mathrm{vac}} \approx a_0^2/2$. We obtain 50 nC for $a_0 = 27$, 30 nC for $a_0 = 60$ and 30 nC for $a_0 = 85$ for the channel density $n_e = 0.01 n_c$. For the channel density of $0.1 n_c$, the total charge exceeds 100 nC for the 10 PW case. The conversion efficiency for our simulations was in the order of tens of percent, see Appendix. The maximum energy increase over time is shown in Fig. 3(b). The maximum energy increases linearly with the propagation distance until saturation and the fastest energy gain is associated with the highest a_0. This is consistent with the previously derived rate for the energy gain over time $d\gamma/dt \sim a_0 \omega_p/\sqrt{I}$ [49]. The energy increase stops at γ_{max} as defined by Eq. (3). This has important implications for experiments: to achieve the theoretical energy limit, the acceleration needs to be sustained for the distance L_{acc}.

The most energetic electrons oscillate with y_{max} around the channel axis, which is visible in Figs. 3(c) and 3(d) that shows the two-dimensional electron histogram in energy and instantaneous distance from the axis. The figures demonstrate that if the laser pulse is not wide enough to interact with electrons at the optimal transverse distance ($W_0 < y_{\mathrm{max}}$), increasing the width W_0 of the laser pulse leads to the increase in electron energy. This indicates that the choice of W_0 was not optimal for the given a_0. The maximum energy at the maximum transverse oscillation distance follows the theoretical prediction for both values of W_0. The highest energies are not located on-axis even though this is the region with the highest intensity because the electrons initially closer to the channel axis have a lower energy limit. Such a dependence of maximum energies on the oscillation amplitude consequently results in the forking structure of the phase space, which is one of the experimental signatures of the DLA [23]. Note that the high-energy electrons close to the $y = 0$ in Fig. 3(c) are in fact electrons with a high y_0 midoscillation.

Choosing the optimal width of the laser pulse is crucial for maximizing electron energies. If the laser pulse is too wide ($W_0 \gg y_{\mathrm{max}}$), the laser energy is used for the interaction with electrons beyond y_{max} that cannot get accelerated by the most efficient first harmonic resonance. On the other hand, if the laser pulse is too narrow, electrons with the potential to achieve the highest energies ($y_0 \approx y_{\mathrm{max}}$) cannot get accelerated. Therefore, the laser pulse is optimally focused when the laser waist and the guiding channel width are matched to the oscillation distance y_{max}. To ensure matched conditions, an optimal focal width for a given laser system can be estimated analytically. We take that the betatron oscillations amplitude should not exceed $y \sim W_0/1.2$, where the amplitude of the electric field is half of the maximum for a Gaussian pulse. This can be expressed in terms of the equation as $W_0/1.2 = y_{\mathrm{max}}(\omega_p, P)$, where the field amplitude a_0 was replaced by the laser power P. The optimal focus is then achieved if the maximum amplitude of betatron oscillations given by the laser width is equal to maximum resonant distance y_{max} expressed by Eq. (2). Preformed guiding channel prevents the laser diffraction and along with the self-focusing sets the upper limit on the laser waist.

Optimal focusing can be prescribed as a function of the laser power given by $P[\mathrm{PW}] \simeq 2.2 \times 10^{-5} a_0^2 W_0^2[\mu\mathrm{m}]/\lambda^2[\mu\mathrm{m}]$. The optimal value of the laser waist W_0 for a given laser power P and the plasma frequency ω_p satisfies the following equation

$$W_0^2[\lambda] = \left(\frac{\omega_0}{\omega_p}\frac{1.2}{\pi}\right)^2 \left[\left(\frac{\omega_p}{\omega_0 \varepsilon_{cr}}\sqrt{\frac{P[\mathrm{PW}]}{2.2\times 10^{-5}}}\right)^{2/3} \frac{1}{W_0^{2/3}[\lambda]} - 1\right]. \tag{4}$$

Equation (4) allows an optimal spotsize for any given laser system to be found, summarized in Fig. 4(a) optical lasers ($\lambda = 1$ μm). The obtained value of optimal spotsize defines the maximum achievable energy shown in Fig. 4(b). At higher density regions, these predictions are corrected due to radiation reaction limit. The corresponding peak a_0 in the case of optimal focus is shown in Fig. 4(c). The calculations reveal the energy electrons can gain is higher for lower plasma densities, but they require a longer acceleration distance as shown in Fig. 4(d). It was found out by Shaw

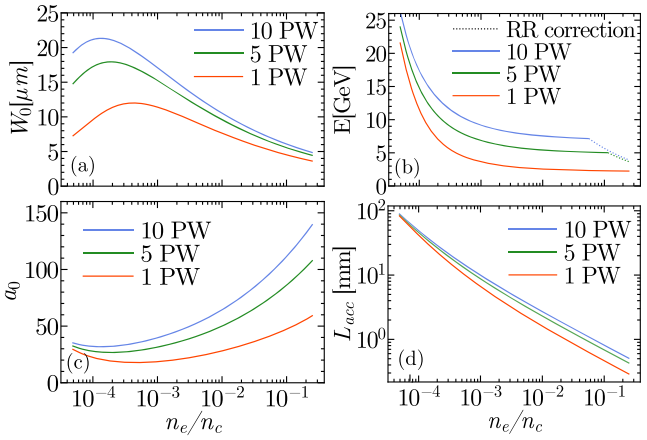

FIG. 4. (a) Optimal focusing of the laser as a function of total power. At the given density, the maximum energy is achieved if the stable propagation of the laser pulse is ensured for long enough. (b) The value of electron energy that should be achieved at ideal focusing of the laser pulse according to values in (a). (c) The value of laser a_0 resulting from the optimal focusing. (d) The acceleration length needed to achieve the maximum predicted energies.

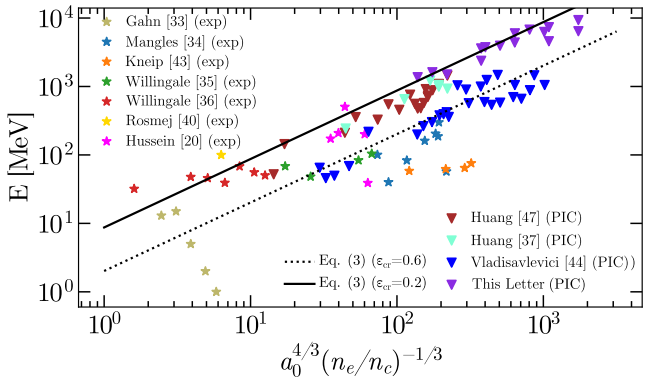

FIG. 5. Comparison of cutoff energies obtained in various experiments and simulations with our scaling Eq. (3). The density is normalized to the critical density. Triangles depict the values obtained from simulations and stars depict experiments.

et al. [22] that the LWFA can contribute to the acceleration process if a significant overlap between the transverse field and trapped electrons is present. This happens if the dimensionless parameter $\omega_p \tau_{\text{laser}}/2\pi a_0 \approx 1$, where τ_{laser} is the laser duration. Such an overlap of both mechanisms can be expected at low plasma densities $n_e < 0.01 n_c$, potentially opening a path towards previously unreached electron energies.

We note that the theoretical predictions presented above neglect effects such as strong self-focusing as well as the nonlinear effects after the injection of many electrons that can alter the background field structure. Furthermore, the value of ε_{cr} influences the value of optimal laser width and consequent electron energies. For the solution in Fig. 4, $\varepsilon_{cr} = 0.2$ was used consistently with the previously discussed scalings, which was also measured in PIC simulations to be close to 0.2 for our conditions. However, the value of ε_{cr} can slightly vary depending on the shape of a preformed channel, injection from channel walls or electron pre-acceleration by the stochastic motion resulting from instabilities present during the propagation. To illustrate the validity of this choice, we have compared predictions of Eq. (3) with the cutoff energies extracted from several experiments and PIC simulations in Fig. 5. This illustrates that the best case scenario obtained so far with no pre-acceleration is $\varepsilon_{cr} = 0.2$, using a wide range of laser intensities and plasma densities, but also that it is not straightforward to achieve these energies, even in simulations. To ensure that the maximum energy corresponding to $\varepsilon = 0.2$ is reached, the propagation distance L_{acc} needs to be ensured and the condition for laser focusing $W_0 \geq y_{\max}$ needs to be fulfilled to enable the acceleration of the most energetic electrons.

In summary, we provide the path towards reaching highest possible energies of electrons in near-critical plasma and gas jets with the next generation of lasers while achieving the high accelerated charge and conversion efficiency. Because of the nature of DLA, the electron energy cutoff depends nontrivially on the laser intensity. Our PIC simulations in quasi-3D geometry demonstrate that the pulse width has a central role in the acceleration process, and they quantitatively agree with the predictions of our analytical model. We have found that for multipetawatt lasers, the best strategy is to use a wide laser focus ($\sim$10 laser wavelengths), low plasma density (around 0.01 n_c), and operate at moderate intensity ($a_0 \sim 60$) as this combination of parameters allows beam energy cutoff $\sim$10 GeV. To obtain this result, it is necessary to ensure a stable propagation of the laser pulse, without a significant reduction of intensity over a few-mm distance. Laser guiding within a preformed plasma channel is a good candidate for accomplishing this. The simulations we presented in this work predict beams with superponderomotive electrons in excess of 100 nC per shot, which can be optimized in further studies.

The authors acknowledge fruitful discussions with Dr. B. Martinez. This work was supported by FCT Grants CEECIND/01906/2018, PTDC/FIS-PLA/3800/2021 DOI: 10.54499/PTDC/FIS-PLA/3800/2021 and FCT UI/BD/151560/2021. We acknowledge use of the Marenostrum (Spain) and LUMI (Finland) supercomputers through PRACE/EuroHPC awards. This work was supported by the Ministry of Education, Youth and Sports of the Czech Republic through the e-INFRA CZ (ID:90140). L. W. and A. A. were supported by the Department of Energy National Nuclear Security Administration under Award No. DE-NA0004030.

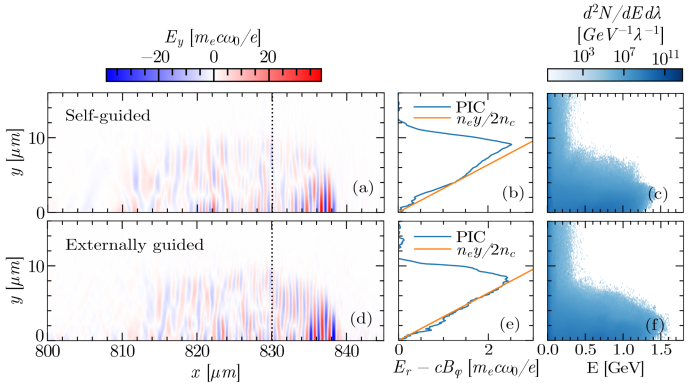

FIG. 6. (a) Snapshot of the laser transverse electric field component at the moment, when electron maximum energies were achieved. (b) Line-out of the transverse ion channel focusing field at $x = 830$ μm compared with the field used in the analytical model. (c) Electron energies as a function of transverse displacement at the moment when the maximum energies were achieved. Panels (a)–(c) depict the evolution in the self-guided regime (transversely constant plasma) and panels (d)–(f) depict the interaction in the externally guided regime with the preformed plasma channel. Simulation parameters are $a_0 = 27$, $W_0 = 8$ μm and $n_e = 0.1n_c$. In the externally guided case the density n_e refers to the plasma density at the channel axis.

Appendix A: Simulation parameters.—Simulations presented in this Letter were performed using particle-in-cell code OSIRIS in quasi-3D geometry. The simulation box was 160 μm long in the laser propagation direction and 40 μm wide in the perpendicular direction. The grid was discretized into $\Delta x \times \Delta y = 9600 \times 864$ of cells. The time step was $\Delta t = 2.55 \times 10^{-17}$ s. The simulations with the wider laser pulse were performed with the same spatial resolution using a wider simulation box (the size was increased in the transverse direction to 71 μm). For both electrons and ions, 32 particles per cell were used. The first two modes of the angular decomposition were used. The axisymmetric mode that resolves the self-generated channel fields and the nonaxisymmetric that describes the linearly polarized laser field.

The transverse plasma density profile in the channel (both the density of electrons and ions) was $n(y)/n_c = n_{\min} + (n_{\max} - n_{\min})(y/r_c)^5$ up to the channel radius distance $r_c = 20$ μm. The n_c corresponds to the critical density for the laser of frequency ω_0 and is defined as $n_c = m\varepsilon_0\omega_0^2/e^2$ where m is the electron mass, e is the electron charge and ε_0 is the vacuum permittivity. Such a channel is defined in a way that $n_{\min}$ is the density in the center of the profile and increases up to $n_{\max} = 2n_c$ at $y = r_c$. At $y > r_c$, the density decreases linearly to $1n_c$. The "channel density" referred throughout the Letter, corresponds to the value of $n_{\min}$ at the centre of the channel (on-axis). The density is uniform along the propagation direction.

The duration of the laser pulse was 200 fs with an envelope defined by the symmetrical polynomial function that rises as $10\tau^3 - 15\tau^4 + 6\tau^5$, where $\tau = \sqrt{2}/\tau_0$ and τ_0 is the pulse duration in FWHM. The transverse laser spotsize was $W_0 = 8$ μm, while transverse dimensionless field amplitude was defined as $a_0(y) = \exp[-y^2/W_0^2]$. The ratio $r_c/W_0 = 2.5$ was kept constant throughout the work, including the simulations with laser pulse $W_0 = 15$ μm. This means that the plasma density profile was adjusted accordingly for the simulations with the wider pulse.

Appendix B: The role of laser guiding by the preformed plasma channel.—The energy scaling law presented in this Letter [Eq. (3)] is valid under the assumption of a sufficiently long and stable propagation distance. In our simulations, this is ensured by a preformed guiding structure provided by a quasineutral plasma channel. However, the laser pulse can guide itself due to the relativistic self-focusing for sufficiently large distances in many scenarios even without external guiding. In Figs. 6(a) and 6(d), the laser pulse is shown for both cases at the moment when the electrons obtain the maximum energy. The simulation parameters for the comparison were: $n_e = 0.1n_c$, $W_0 = 8$ μm, and $a_0 = 27$. After nearly a 1 mm of propagation, the laser shape and the intensity profile in both cases are comparable. The Figs. 6(b) and 6(e) shows the ion channel field structure. The transverse dependence of the quasistatic electric and magnetic fields responsible for the betatron oscillations are almost identical for the self-guided and the externally guided scenario. It is also worth noting the agreement of the field observed in the PIC simulations with the dependence used in the analytical model $E_r \sim n_e r/2n_c$. The separation of the laser field and the channel field was possible due to the azimuthal decomposition of the fields [58]. Panels (c) and (f) compare the electron 2D histogram, which is a function of transverse distance and the electron energy, with no appreciable difference noted. Even though the laser pulse can propagate for sufficiently long distances due to the self-focusing, the external guiding allows us to have better control over the laser

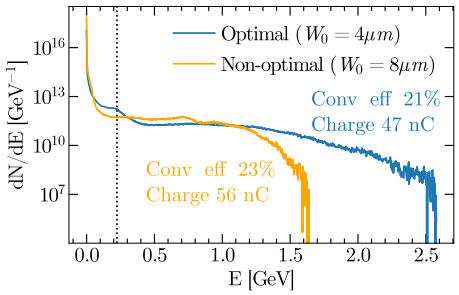

FIG. 7. Distribution function of electrons accelerated by the 1PW laser pulse focused optimally and slightly off optimal focusing interacting with the plasma of density $0.1n_c$. The channel spotsize was controlled by the pre-formed plasma guiding channel, which resulted in $a_0 = 27$ for the case with $W_0 = 8$ μm and $a_0 = 54$ for the case with $W_0 = 4$ μm.

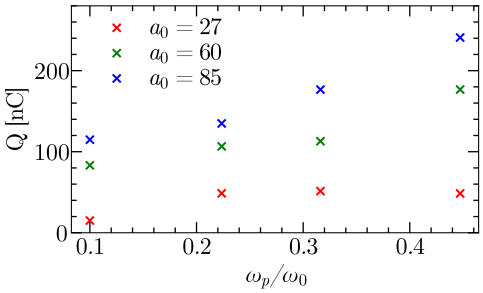

FIG. 8. Total electron charge with energies exceeding 300 MeV obtained in simulations with different plasma frequencies and laser intensities. The total charge was extracted at the moment when the maximum energy in the simulation was achieved.

spot size during the propagation. This enables the laser pulse propagation with laser spot size matched to the maximum transverse resonant distance, resulting in the most optimal DLA.

Appendix C: The energy conversion efficiency at the optimal scenario.—The reader might wonder why we focused on optimizing the cutoff energy rather than the energy conversion efficiency. In fact, as shown in Fig. 7, the optimal focusing and nonoptimal focusing examples have comparable conversion efficiency into hot electrons with energies over 220 MeV (21% and 23%). Both simulations were performed for the 1 PW laser, externally guided and focused to different spot sizes. One simulation (nonoptimal) was performed with the laser pulse focused to $W_0 = 8$ μm with $a_0 = 27$. In the other simulation [optimal according to Eq. (4)] the laser pulse was focused to $W_0 = 4$ μm with $a_0 = 54$. We can see that the optimal focusing led to the increase in the cutoff energy from 1.6 to 2.6 GeV, while the total accelerated charge is decreased by 16% and conversion efficiency has changed only by a few percent. The energy conversion efficiency is therefore not compromised by our optimization focused on the cutoff energy.

It might be tempting to expect the energy conversion efficiency to be lower for low plasma densities, which are found optimal in terms of energy cutoff. This is not the case, because the DLA can be highly efficient even if the plasma density is decreased. For example, a simulation at an order of magnitude lower density $n_e = 0.01n_c$, $W_0 = 8$ μm, and $a_0 = 27$ (1 PW) resulted in 50 nC of accelerated charge, which is comparable to the results with $0.1n_c$ mentioned above. The reason is the difference in the total interaction time. As the energy gain over time is slower at lower plasma densities, the propagation time (and, consequently, the propagation distance) is longer. Since the total injected charge increases linearly with time [62], a lower plasma density does not automatically decrease the total accelerated charge or the energy efficiency. In fact, it has been experimentally demonstrated that the plasma density on the order of 10^{18}–10^{19} cm^{-3} can result in a high total charge of hundreds of nC [20,21].

Appendix D: The charge injection.—According to our scaling, multi-GeV energies are expected at low plasma densities. It has been previously demonstrated, that the accelerated charge increases with the propagation distance [62]. As laser propagates, electrons are captured from the side at the laser pulse boundary or at the front of the pulse and the quasistatic fields of the ion channel capture those electrons along the axis of laser propagation. The longer laser propagates, the more charge can get injected. Therefore, laser propagation over several millimeters can compensate the slow electron injection rate resulting in a very high total charge. The total injected charge for various plasma frequencies and laser intensities is shown in Fig. 8. The data points correspond to the same simulations as those in Fig. 2(c). All presented simulations are with the same spotsize (of 8 microns) for simplicity of comparison. The total charge was taken at the moment when the injected charge in the simulation reached the maximum. We have included only electrons with energies exceeding 300 MeV. Note that the moment corresponding to the maximum total charge is not identical to the moment when electrons reach the maximum energy. In general, the charge injection can be happening even after the maximum energy is reached.

Several conclusions can be drawn from Fig. 8. The total charge increases with the laser intensity a_0 and plasma density (represented by the plasma frequency ω_p). A deeper analysis of the performed simulations reveals that the injection rate depends on the field amplitude a_0 and plasma frequency ω_p, which then affects the total charge. One should expect the injection rate also to depend on the laser spotsize W_0 and the laser duration, since they influence the total area of the laser-dense plasma interface that determines the amount of available electrons. Obtaining a scaling for the total accelerated charge will be a subject of our future work. Nonetheless, from these

results, one can conclude, that the direct laser acceleration by multi-PW lasers in underdense gas targets is capable of providing electron bunches with a total charge of tens or hundreds of nC.

*robert.babjak@tecnico.ulisboa.pt

[1] J. Faure, Y. Glinec, A. Pukhov, S. Kiselev, S. Gordienko, E. Lefebvre, J. P. Rousseau, F. Burgy, and V. Malka, Nature (London) **431**, 541 (2004).

[2] C. G. R. Geddes, C. Toth, J. van Tilborg, E. Esarey, C. B. Schroeder, D. Bruhwiler, C. Nieter, J. Cary, and W. P. Leemans, Nature (London) **431**, 538 (2004).

[3] S. P. D. Mangles, C. D. Murphy, Z. Najmudin, A. G. R. Thomas, J. L. Collier, A. E. Dangor, E. J. Divall, P. S. Foster, J. G. Gallacher, C. J. Hooker, D. A. Jaroszynski, A. J. Langley, W. B. Mori, P. A. Norreys, F. S. Tsung, R. Viskup, B. R. Walton, and K. Krushelnick, Nature (London) **431**, 535 (2004).

[4] W. P. Leemans, A. J. Gonsalves, H.-S. Mao, K. Nakamura, C. Benedetti, C. B. Schroeder, C. Tóth, J. Daniels, D. E. Mittelberger, S. S. Bulanov, J.-L. Vay, C. G. R. Geddes, and E. Esarey, Phys. Rev. Lett. **113**, 245002 (2014).

[5] A. J. Gonsalves *et al.*, Phys. Rev. Lett. **122**, 084801 (2019).

[6] S. Chen, N. D. Powers, I. Ghebregziabher, C. M. Maharjan, C. Liu, G. Golovin, S. Banerjee, J. Zhang, N. Cunningham, A. Moorti, S. Clarke, S. Pozzi, and D. P. Umstadter, Phys. Rev. Lett. **110**, 155003 (2013).

[7] D. J. Stark, T. Toncian, and A. V. Arefiev, Phys. Rev. Lett. **116**, 185003 (2016).

[8] O. Jansen, T. Wang, D. J. Stark, E. d'Humières, T. Toncian, and A. V. Arefiev, Plasma Phys. Control. Fusion **60**, 054006 (2018).

[9] M. M. Günther, O. N. Rosmej, P. Tavana, M. Gyrdymov, A. Skobliakov, A. Kantsyrev, S. Zähter, N. G. Borisenko, A. Pukhov, and N. E. Andreev, Nat. Commun. **13**, 170 (2022).

[10] R. A. Snavely, M. H. Key, S. P. Hatchett, T. E. Cowan, M. Roth, T. W. Phillips, M. A. Stoyer, E. A. Henry, T. C. Sangster, M. S. Singh, S. C. Wilks, A. MacKinnon, A. Offenberger, D. M. Pennington, K. Yasuike, A. B. Langdon, B. F. Lasinski, J. Johnson, M. D. Perry, and E. M. Campbell, Phys. Rev. Lett. **85**, 2945 (2000).

[11] S. C. Wilks, A. B. Langdon, T. E. Cowan, M. Roth, M. Singh, S. Hatchett, M. H. Key, D. Pennington, A. MacKinnon, and R. A. Snavely, Phys. Plasmas **8**, 542 (2001).

[12] H. Chen, S. C. Wilks, J. D. Bonlie, E. P. Liang, J. Myatt, D. F. Price, D. D. Meyerhofer, and P. Beiersdorfer, Phys. Rev. Lett. **102**, 105001 (2009).

[13] M. Vranic, O. Klimo, G. Korn, and S. Weber, Sci. Rep. **8**, 4702 (2018).

[14] Y. He, I.-L. Yeh, T. G. Blackburn, and A. Arefiev, New J. Phys. **23**, 115005 (2021).

[15] Y. He, T. G. Blackburn, T. Toncian, and A. V. Arefiev, Commun. Phys. **4**, 139 (2021).

[16] Ó. Amaro and M. Vranic, New J. Phys. **23**, 115001 (2021).

[17] B. Martinez, B. Barbosa, and M. Vranic, Phys. Rev. Accel. Beams **26**, 011301 (2023).

[18] A. Pukhov and J. Meyer-ter Vehn, Phys. Plasmas **5**, 1880 (1998).

[19] A. Pukhov, Z.-M. Sheng, and J. Meyer-ter Vehn, Phys. Plasmas **6**, 2847 (1999).

[20] A. E. Hussein, A. V. Arefiev, T. Batson, H. Chen, R. S. Craxton, A. S. Davies, D. H. Froula, Z. Gong, D. Haberberger, Y. Ma, P. M. Nilson, W. Theobald, T. Wang, K. Weichman, G. J. Williams, and L. Willingale, New J. Phys. **23**, 023031 (2021).

[21] J. L. Shaw, M. A. Romo-Gonzalez, N. Lemos, P. M. King, G. Bruhaug, K. G. Miller, C. Dorrer, B. Kruschwitz, L. Waxer, G. J. Williams, M. V. Ambat, M. M. McKie, M. D. Sinclair, W. B. Mori, C. Joshi, H. Chen, J. P. Palastro, F. Albert, and D. H. Froula, Sci. Rep. **11**, 7498 (2021).

[22] J. L. Shaw, N. Lemos, L. D. Amorim, N. Vafaei-Najafabadi, K. A. Marsh, F. S. Tsung, W. B. Mori, and C. Joshi, Phys. Rev. Lett. **118**, 064801 (2017).

[23] J. L. Shaw, N. Lemos, K. A. Marsh, D. H. Froula, and C. Joshi, Plasma Phys. Control. Fusion **60**, 044012 (2018).

[24] P. M. King, K. Miller, N. Lemos, J. L. Shaw, B. F. Kraus, M. Thibodeau, B. M. Hegelich, J. Hinojosa, P. Michel, C. Joshi, K. A. Marsh, W. Mori, A. Pak, A. G. R. Thomas, and F. Albert, Phys. Rev. Accel. Beams **24**, 011302 (2021).

[25] M. Lamač, U. Chaulagain, L. Jurkovičová, J. Nejdl, and S. V. Bulanov, Phys. Rev. Res. **3**, 033088 (2021).

[26] K. G. Miller, J. P. Palastro, J. L. Shaw, F. Li, F. S. Tsung, V. K. Decyk, C. Joshi, and W. B. Mori, Phys. Plasmas **30**, 073902 (2023).

[27] I. Cohen, T. Meir, K. Tangtartharakul, L. Perelmutter, M. Elkind, Y. Gershuni, A. Levanon, A. V. Arefiev, and I. Pomerantz, Sci. Adv. **10**, eadk1947 (2024).

[28] C. Aniculaesei *et al.*, Matter Radiat. Extremes **9**, 014001 (2024).

[29] J. Zou, C. Le Blanc, D. Papadopoulos, G. Chériaux, P. Georges, G. Mennerat, F. Druon, L. Lecherbourg, A. Pellegrina, P. Ramirez *et al.*, High Power Laser Sci. Eng. **3**, e2 (2015).

[30] S. Weber *et al.*, Matter Radiat. Extremes **2**, 149 (2017).

[31] K. A. Tanaka *et al.*, Matter Radiat. Extremes **5**, 024402 (2020).

[32] H. G. Rinderknecht, T. Wang, A. L. Garcia, G. Bruhaug, M. S. Wei, H. J. Quevedo, T. Ditmire, J. Williams, A. Haid, D. Doria, K. M. Spohr, T. Toncian, and A. Arefiev, New J. Phys. **23**, 095009 (2021).

[33] C. Gahn, G. D. Tsakiris, A. Pukhov, J. Meyer-ter Vehn, G. Pretzler, P. Thirolf, D. Habs, and K. J. Witte, Phys. Rev. Lett. **83**, 4772 (1999).

[34] S. P. D. Mangles, B. R. Walton, M. Tzoufras, Z. Najmudin, R. J. Clarke, A. E. Dangor, R. G. Evans, S. Fritzler, A. Gopal, C. Hernandez-Gomez, W. B. Mori, W. Rozmus, M. Tatarakis, A. G. R. Thomas, F. S. Tsung, M. S. Wei, and K. Krushelnick, Phys. Rev. Lett. **94**, 245001 (2005).

[35] L. Willingale, A. G. Thomas, P. M. Nilson, H. Chen, J. Cobble, R. S. Craxton, A. Maksimchuk, P. A. Norreys, T. C. Sangster, R. H. Scott, C. Stoeckl, C. Zulick, and K. Krushelnick, New J. Phys. **15**, 025023 (2013).

[36] L. Willingale, A. V. Arefiev, G. J. Williams, H. Chen, F. Dollar, A. U. Hazi, A. Maksimchuk, M. J.-E. Manuel, E. Marley, W. Nazarov, T. Z. Zhao, and C. Zulick, New J. Phys. **20**, 093024 (2018).

[37] T. W. Huang, C. T. Zhou, H. Zhang, S. Z. Wu, B. Qiao, X. T. He, and S. C. Ruan, Phys. Rev. E **95**, 043207 (2017).
[38] O. N. Rosmej, N. E. Andreev, S. Zaehter, N. Zahn, P. Christ, B. Borm, T. Radon, A. Sokolov, L. P. Pugachev, D. Khaghani, F. Horst, N. G. Borisenko, G. Sklizkov, and V. G. Pimenov, New J. Phys. **21**, 043044 (2019).
[39] O. N. Rosmej, M. Gyrdymov, M. M. Günther, N. E. Andreev, P. Tavana, P. Neumayer, S. Zähter, N. Zahn, V. S. Popov, N. G. Borisenko, A. Kantsyrev, A. Skobliakov, V. Panyushkin, A. Bogdanov, F. Consoli, X. F. Shen, and A. Pukhov, Plasma Phys. Control. Fusion **62**, 115024 (2020).
[40] O. N. Rosmej, X. F. Shen, A. Pukhov, L. Antonelli, F. Barbato, M. Gyrdymov, M. M. Günther, S. Zähter, V. S. Popov, N. G. Borisenko, and N. E. Andreev, Matter Radiat. Extremes **6**, 048401 (2021).
[41] D. R. Rusby *et al.*, Phys. Plasmas **30**, 023103 (2023).
[42] I. M. Vladisavlevici, D. Vizman, and E. d'Humières, Plasma Phys. Control. Fusion **65**, 045012 (2023).
[43] S. Kneip *et al.*, Phys. Rev. Lett. **100**, 105006 (2008).
[44] I.-M. Vladisavlevici, D. Vizman, and E. d'Humières, Photonics **9**, 953 (2022).
[45] V. Khudik, A. Arefiev, X. Zhang, and G. Shvets, Phys. Plasmas **23**, 103108 (2016).
[46] A. V. Arefiev, B. N. Breizman, M. Schollmeier, and V. N. Khudik, Phys. Rev. Lett. **108**, 145004 (2012).
[47] T. W. Huang, A. P. L. Robinson, C. T. Zhou, B. Qiao, B. Liu, S. C. Ruan, X. T. He, and P. A. Norreys, Phys. Rev. E **93**, 063203 (2016).
[48] T. W. Huang, C. T. Zhou, A. P. L. Robinson, B. Qiao, A. V. Arefiev, P. A. Norreys, X. T. He, and S. C. Ruan, Phys. Plasmas **24**, 043105 (2017).
[49] M. Jirka, M. Vranic, T. Grismayer, and L. O. Silva, New J. Phys. **22**, 083058 (2020).
[50] A. V. Arefiev, V. N. Khudik, A. P. L. Robinson, G. Shvets, L. Willingale, and M. Schollmeier, Phys. Plasmas **23**, 056704 (2016).
[51] A. V. Arefiev, V. N. Khudik, A. P. L. Robinson, G. Shvets, and L. Willingale, Phys. Plasmas **23**, 023111 (2016).
[52] M. Vranic, R. A. Fonseca, and L. O. Silva, Plasma Phys. Control. Fusion **60**, 034002 (2018).
[53] A. Pukhov, Rep. Prog. Phys. **66**, 47 (2002).
[54] A. V. Arefiev, V. N. Khudik, and M. Schollmeier, Phys. Plasmas **21**, 033104 (2014).
[55] I.-L. Yeh, K. Tangtartharakul, H. G. Rinderknecht, L. Willingale, and A. Arefiev, New J. Phys. **23**, 095010 (2021).
[56] T. Wang, V. Khudik, A. Arefiev, and G. Shvets, Phys. Plasmas **26**, 083101 (2019).
[57] R. A. Fonseca, L. O. Silva, F. S. Tsung, V. K. Decyk, W. Lu, C. Ren, W. B. Mori, S. Deng, S. Lee, T. Katsouleas, and J. C. Adam, in *Computational Science—ICCS 2002*, edited by P. M. A. Sloot, A. G. Hoekstra, C. J. K. Tan, and J. J. Dongarra (Springer Berlin Heidelberg, Berlin, Heidelberg, 2002), pp. 342–351.
[58] A. Davidson, A. Tableman, W. An, F. Tsung, W. Lu, J. Vieira, R. Fonseca, L. Silva, and W. Mori, J. Comput. Phys. **281**, 1063 (2015).
[59] T. Levato, M. Nevrkla, M. F. Nawaz, L. Giuffrida, F. Grepl, H. Zulic, J. Pilar, M. Hanus, M. Divoky, A. Lucianetti, T. Mocek, and D. Margarone, Appl. Sci. **10**, 4082 (2020).
[60] K. Oubrerie, A. Leblanc, O. Kononenko, R. Lahaye, I. A. Andriyash, J. Gautier, J.-P. Goddet, L. Martelli, A. Tafzi, K. Ta Phuoc, S. Smartsev, and C. Thaury, Light Sci. Appl. **11**, 180 (2022).
[61] D. N. Gupta, S. R. Yoffe, A. Jain, B. Ersfeld, and D. A. Jaroszynski, Sci. Rep. **12**, 20368 (2022).
[62] P. Valenta, D. Mašlárová, R. Babjak, B. Martinez, S. V. Bulanov, and M. Vranić, in *Research Using Extreme Light: Entering New Frontiers with Petawatt-Class Lasers V*, edited by S. V. Bulanov and L. O. Silva, International Society for Optics and Photonics Vol. 12580 (SPIE, 2023), p. 1258002.